


## Limitations for field-enhanced atom interferometry

D. Comparat 

*Université Paris-Saclay, CNRS, Laboratoire Aimé Cotton, 91405, Orsay, France*

 (Received 1 September 2019; revised manuscript received 22 December 2019; accepted 22 January 2020; published 14 February 2020)

We discuss the possibility to enhance the sensitivity of optical interferometric devices by increasing their open area using an external field gradient that acts differently on the two arms of the interferometers. The use of a combined electric and magnetic field cancels nonlinear terms that dephase the interferometer. This is possible using well-defined (typically with  $n \sim 20$  Rydberg) states, a magnetic field of a few Tesla, and an electric field gradient of  $\sim 10$  V/cm<sup>2</sup>. However, this allows for interaction times only on the order of tens of microseconds, leading to a reachable accuracy of only 1 or 2 orders of magnitude higher than standard light-pulse atom interferometers. Furthermore, the control of fields and states and three-dimensional (3D) trajectories puts severe limits to the reachable accuracy. This idea is therefore not suitable for precision measurement but might eventually be used for gravity or neutrality in antimatter studies.

DOI: [10.1103/PhysRevA.101.023606](https://doi.org/10.1103/PhysRevA.101.023606)

### I. INTRODUCTION

The effect of an external force (gravitation on neutral particles, or electric and magnetic force on non-neutral particles) can be accurately measured using the phase acquired in the potential of a suitably built interferometer, such as demonstrated, for instance, in the classic Colella Overhauser Werner's experiment [1]. Nowadays, most of the interferometers are based on mechanical gratings or optical manipulation of internal states using gratings such as Mach-Zehnder [2,3], Moiré [4], or Talbot(-Lau) [3,5,6]. Taking the gravity measurement as a generic example, the rms statistical precision  $\delta g$  on the measurement of the  $g$  value is quite generally estimated [2] as  $\frac{\delta g}{g} = \frac{1}{C\sqrt{N_{\text{det}}}} \frac{1}{\phi}$ , where  $\phi$  is the phase difference between the paths in the interferometer.  $C \leq 1$  is the fringe contrast and  $N_{\text{det}}$  the number of events detected. In light-pulse atom interferometry, the light gratings are applied at well-defined times (for instance,  $0, \frac{T}{2}, T$ ); therefore, the phase shift becomes independent of the atom velocity. For mechanical grating, with  $d$  the grating pitch, the interferometric phase shift  $\phi$  is given by  $\frac{d}{2} \frac{\phi}{2\pi} = \frac{1}{2} g T^2$ , and the contrast of such interferometry can approach unity (the difficulty becomes now to catch all atoms by the laser pulses) [2]. The sensitivity of these devices increases with the measured phase difference between the matter waves  $\phi = \frac{m}{\hbar} A \cdot g$ , which scales with the enclosed interferometric area in space-time  $A = \int \Delta x dt$ . Increasing the area is therefore the key ingredient to improve accuracy. In most of the interferometer (Ramsey-Brodé [7] or Kasevitch-Chu [8] type) the atomic beams are coherently split and later recombined using laser-pulse beam splitters that transfer photon momentum  $\hbar k$  ( $k = 2\pi/\lambda$  is the light wave vector for a wavelength  $\lambda$  that plays the role of the grating pitch  $d$ ) [9,10]. In order to increase the area, large momentum transfer interferometers have been demonstrated with  $A = 2N \int t \hbar k / m dt = NT^2 \hbar k / m$  using  $N$  photon transfers from the laser beams. Many methods are now available [10], typically limited to  $N \sim 100$ , such as Kapitza-Dirac [11],

Talbot-Lau [12,13], sequential Raman pulses [14], sequential two-photon Bragg diffraction [15], multiphoton Bragg diffraction [16], Bloch oscillations [17,18], or adiabatic passage [19].

In this article we would like to study another possibility, which is to increase the area  $A$  by using an external field acting differently on the two arms of the interferometer. A proof-of-principle experiment has been realized in [20] (see also [21–23]) by the use of an external magnetic field gradient. Theoretically, only the simple ideal (pure gradient) one-dimensional case has been studied in Refs. [24,25]. A simple comparison can be done between this enhanced interferometer, based on external electromagnetic accelerations  $a$  where  $A \approx \int a t^2 / 2 dt \approx a T^3 / 6$ , and a pure photon-recoil-based light interferometer, with  $A = T^2 \hbar k / m$ . The gain exists only when  $aT \gg \hbar k / m$  so, with  $a$  very big and for a long interrogation time  $T$ . For a typical wavelength of  $\lambda = 532$  nm and for hydrogen mass atoms, this leads to  $aT \gg 1$  m/s. Because strong acceleration can be created, for instance, in Rydberg states under the effect of an electric field, the gain is potentially enormous. For instance (see detailed formula in the Appendix), a Rydberg state of  $n \sim 30$  and an electric field gradient of 100 V/mm<sup>2</sup> leads to a gain  $\sim 10^5$  on  $\delta g/g$  compared to a standard interferometer even for very short interrogation times of  $T = 100 \mu\text{s}$ . Furthermore, with lower temperature, such as that achieved thanks to laser cooling [26,27], the interrogation time can be longer and the gain potentially much bigger. The enhanced interferometer has a  $T^3$  evolution compared to the  $T^2$  evolution of a standard interferometer, explaining why such an enhanced gradient interferometer has seemed to be so promising [21–24,28,29].

In our study, we will first express some experimental considerations of such gradient-enhanced interferometry and show that it is not suitable for precision measurements but may be interesting for experiments having high temperature and low statistics, such as antimatter experiments. We then first study the one-dimensional (1D) case and second a real

three-dimensional (3D) case but in a simple cylindrical symmetry. We will show that, due to Maxwell's equations, the 3D case leads to extra terms in the phase that seem difficult to cancel. This leads to difficulties that will strongly limit the possible gain.

## II. EXPERIMENTAL CONSIDERATIONS

### A. Stability of the fields

For the following we assume that we can use electric and/or magnetic external fields to act on the states. We first stress the realization that a precision experiment using an external field gradient appears very challenging because the degree of control of the time and space values of the applied fields have to be of the same order of magnitude than the relative accuracy foreseen for  $\delta g$ . Because a magnetic or electric field relative spatial homogeneity, or time stability, on the  $10^{-5}$  range may already be seen challenging, an accuracy of  $|\delta g/g| \approx 10^{-5}$  seems already quite hard to achieve. This is in stringent contrast to photon-recoil-based optical interferometers used for high-accuracy measurements where all quantities  $T$ ,  $k$ , and  $m$  can be known at very high accuracy. But if  $|\delta g/g| \approx 10^{-5}$  is well below the state-of-the-art  $|\delta g/g| \approx 10^{-9}$  accuracy for matter waves, it will present a tremendous improvement for antimatter waves, the state of the art of which is  $|\delta g/g| \approx 100$  [9,10,30–37].

### B. Interest for antimatter systems

Therefore such a gradient interferometer may be used to study neutral antimatter systems such as antihydrogen  $\bar{H} = \bar{p} - e^+$ , positronium  $\text{Ps} = e^+ - e^-$ , protonium  $\text{Pn} = \bar{p} - p$ , antiprotonic helium, their muonic counterpart, antineutrons, etc., which, indeed, attracts more and more attention for tests of Lorentz,  $CPT$  invariance [38–42], gravity [43–49], or even for spectroscopic measurement [50]. Proposal of antimatter studies using interferometry dates back to the 1990s [51–53]. Most proposals are based on imaging a first grating by a second one and then detecting the particles either using a third grating or a position-sensitive detector. The gratings method has advantages regardless of the coherence of the source [54]. That is another advantage for antimatter systems because of the low production rate and high temperature of the antimatter samples, meaning extended sources, large beam divergence, and poor energy definition.

The interrogation time  $T$  is strongly related to the temperature  $T_0$  of the atoms. Indeed, the particles will stay in the (laser waist or apparatus) size  $w$  typically on the centimeter scale only during a time  $T \approx w \sqrt{m/k_B T_0}$ . For hydrogen at 1 K this leads to time in the 100- $\mu\text{s}$  range. This implies the use of long-lived states such as ground hyperfine,  $2s$  or  $nl$  Rydberg states (lifetime  $\approx 10^{-10} n^3 (l + 1/2)^2 \text{ s}$  [55]). For such states the typical acceleration verifies  $ma \sim \mu_B m_F \nabla B$  in a magnetic field  $B$ , with  $\mu_B$  the Bohr magneton and  $m_F$  the total magnetic quantum number. Thus, the  $aT \gg 1 \text{ m/s}$  condition indicates that the enhanced interferometer has increased performances compared to a light interferometer, as the one proposed in [2,3], only with a (for hydrogen mass)  $m_F \nabla B \gg 1 \text{ T/m}$  magnetic field gradient or  $n^2 \nabla F \approx 10^6 \text{ V/m}^2$  for the electric

field. Both conditions seem easy to achieve and it is therefore worth investigating the setup in more detail.

### C. Simple example: 1D picture, pure gradient acting in a two-arm interferometer

Even if we see that such a poorly accurate interferometer will interest mostly only the antimatter community, our study of a gradient-enhanced area interferometer will be more general. We focus our general discussion on a simple two-arm interferometer for the sake of simplicity, but most of the discussion would be relevant for multiple arms or multiple gratings. Different forces acting on the two arms of the interferometer requires at least two different internal states  $|1\rangle$  and  $|2\rangle$  on which the external field produces different accelerations  $a_1$  and  $a_2$ . The force acting differentially on both states will create two well spatially separated arms [31,56] with spatial and internal states entangled. This has to be compared to the Talbot-Lau setup or the classical moiré deflectometer, where this entanglement does not exist and so the final measurement has to be spatially resolved. In our case, the final measurement at the output of the interferometer can be performed by a simple internal state measurement. This allows us to work with hotter beams and smaller spatial displacement compared to a single internal state interferometer [3].

The simplest example uses two classical trajectory paths (the internal state can change along the path) through the interferometer with phase evolutions  $\phi_1$  and  $\phi_2$ , where the fringe phase shift will be given by  $\Delta\phi = \phi_1 - \phi_2$ . As studied in Refs. [23,24], the simplest ideal case uses a 1D picture with a pure field gradient  $E$  [electric or magnetic with  $E = \|\mathbf{E}\| = E_0 + E'(z - z_0)$ ] and a linear field dependence on the potential energy [ $E_p(E) = E_p(E_0) + E'_p(E_0)(E - E_0)$  for a given state]. This creates uniform, nonspatial neither time-dependent acceleration  $\tilde{a}_1$  and  $\tilde{a}_2$  with  $\tilde{a}_i = E'E'_{\text{pot}_i}(E_0)/m$ . So including the gravity, the two internal states  $|1\rangle$  and  $|2\rangle$  have different accelerations,  $a_1 = g + \tilde{a}_1$  and  $a_2 = g + \tilde{a}_2$ .

To close in phase space the interferometer, several timings and accelerations are possible. Choosing one solution or the other does not change the conclusions we are going to derive. One possible solution is given in Ref. [21], where (forgetting the gravity) the acceleration of the upper part is  $\tilde{a}, -\tilde{a}, 0, 0$  and  $0, 0, \tilde{a}, -\tilde{a}$  for the lower path, leading to  $\Delta\phi = -\frac{m}{\hbar} g a T^3/32$ , where  $T$  is the total time spent in the interferometer. This solution uses three different accelerations, so in principle three different internal states. Therefore, we will use here the simpler solution proposed in Ref. [24] and recently realized in Ref. [23] (with the  $\pi$  pulse being replaced by field reversals), because it only requires two accelerations  $\tilde{a}_1$  and  $\tilde{a}_2$ . Following [24] we will thus create (by a  $\pi/2$  pulse) the superposition at time 0 and then changing states ( $\pi$  pulse) at time  $T/4, 3T/4$  and recombining ( $\pi/2$  pulse) at  $T$ , as illustrated in the upper panel of Fig. 1.

This choice closes the interferometer both in position and velocity, meaning that the classical path  $\Gamma$  linking the initial to the final point, through Newton's classical trajectories equation  $m\ddot{x}_i + \frac{\partial E_p}{\partial x_i} = 0$ , ends at the same phase-space position for both arms [24]. The phase imprinted by the lasers is  $\phi_L = \phi_L(0) - 2\phi_L(T/4) + 2\phi_L(3T/4) - \phi_L(T)$  [24,57]. Because it is zero if we are assuming no phase jump (coherent laser), we

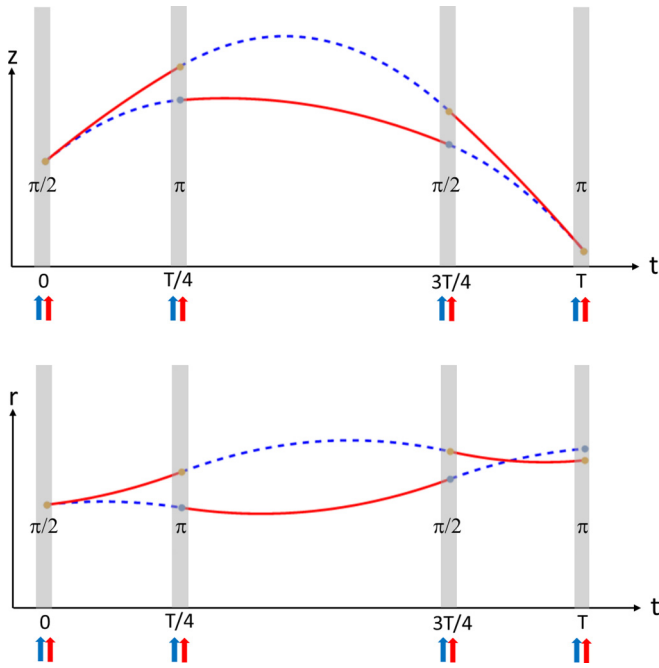


FIG. 1. Space-time diagram of the gradient-enhanced interferometer with four (short and copropagating Raman) laser pulses at time  $0, T/4, 3T/4, T$ . The two internal states are respectively shown in solid-red and dashed-blue curves. If seen as a pure 1D interferometer, a pure gradient interferometer can be closed in the  $z$  coordinate (upper panel). However, when looking to 3D, or with nonlinear terms, the situation is more complex, as shown for the radial coordinate  $r$  (lower panel).

will neglect it in the following. Thus, in this simple case the calculation of the phase evolution [see Eq. (2) detailed later] is straightforward and leads to  $\Delta\phi = \frac{m}{\hbar}(a_1^2 - a_2^2)T^3/64 = -g\frac{m}{\hbar}(\tilde{a}_1 - \tilde{a}_2)T^3/32 + \frac{m}{\hbar}(\tilde{a}_1^2 - \tilde{a}_2^2)T^3/64$ . This formula confirms that, in addition to the desired gravity-dependent phase, another global phase, insensitive to gravity, arises. Because we want the gravity term to be large, we want the accelerations to be large and thus this second phase can also be quite large. Using  $\tilde{a}_1 \approx -\tilde{a}_2$  limits the value of this extra phase. However, without specific tricks it will be difficult to perfectly ensure this equality experimentally, because  $\tilde{a}_1$  and  $\tilde{a}_2$  are sensitive to field fluctuations. Consequently, the field fluctuations will either reduce the contrast or even blur (if this extra phase is bigger than  $2\pi$ ) the interferometer.

#### D. Real 3D case

In addition to this important difficulty, another problem exists. Indeed, the 1D picture is clearly not adequate because Maxwell's equation (or Gauss's law) implies that an electric or magnetic field gradient acts on a multidimensional space. Therefore the electromagnetic force created by an external field gradient is necessary acting on at least two directions. This is important because to keep a good contrast, the trajectories, and so the area, have to be the same for all initial positions and velocities. This can be achieved, for instance, if the particles are submitted to a force that does not depend on positions or on velocities. As we will see, when combined

with the nonlinearity of the Stark or Zeeman effect, this puts strong limits on the states and fields that could be chosen.

Maxwell's equations for static electric and magnetic fields in vacuum have the exact same form so we can treat both fields in the same way. We shall thus first, for simplicity, use an electric field and a simple cylindrical symmetry along the vertical  $z$  axis. From the sole voltage along the axis  $V(z)$ , Maxwell's equations imply a single solution for the 3D potential (in cylindrical coordinates)  $V(\rho, z)$ . Indeed, using series notations  $V(z) = V_0 - E_0z - E'z^2/2 - E''z^3/6 - \dots$  we find [58]

$$V(\rho, z) = V_0 - E_0z - E'z^2/2 - E''z^3/6 + 1/4r^2(E' + E''z) + \dots$$

The gradient gives the electric field  $\mathbf{E}$ . Taking the series (in  $E_0$  or similarly in  $r, z$ ), up to the third order, for the norm  $E = \|\mathbf{E}\|$  leads to

$$E = E_0 + E'z + \frac{E''}{2}z^2 + \frac{E'^2 - 2E_0E''}{8E_0}r^2 - E'\frac{E'^2 - 2E_0E''}{8E_0^2}zr^2.$$

Similarly, the potential energy can be written in series,

$$E_p(E) = E_p(E_0) + E'_p(E - E_0) + \frac{1}{2}E''_p(E - E_0)^2 + \frac{1}{6}E'''_p(E - E_0)^3,$$

where we have noted  $E'_p$  for  $\frac{dE_p}{dE}(E_0)$ . Finally, up to the third order, the Lagrangian becomes

$$L = \frac{p_z^2}{2m} + \frac{p_r^2}{2m} - E_p(E_0) - E'_pE'z - mgz - \frac{E'_pE'' + E''_pE'^2}{2}z^2 - E'_p\frac{E'^2 - 2E_0E''}{8E_0}r^2 - E'\frac{E'^2 - 2E_0E''}{8E_0^2}(E''_pE_0 - E'_p)r^2z - \frac{E'''_pE'^3 + 3E''_pE'E''}{6}z^3. \quad (1)$$

To calculate the phase evolution, we will separate this full Lagrangian  $L(\mathbf{x}, \dot{\mathbf{x}}, t) = \frac{1}{2}m\dot{\mathbf{x}}^2 - E_p(\mathbf{x}, t)$  between a quadratic Lagrangian  $L_0$  containing only homogeneous acceleration and its gradient [so the first two lines of Eq. (1)], and a perturbative Lagrangian  $L_1$  containing only the third-order terms ( $r^2z$  and  $z^3$ ). As recalled in the Appendix, see Eqs. (C1) and (C2), if  $L_1$  is a perturbation, the evaluation of the total phase under the  $L$  Lagrangian can be evaluated using only the classical unperturbed path  $\Gamma_0$  derived with the sole  $L_0$  Lagrangian:

$$\phi = \frac{1}{\hbar} \int_{\Gamma_0} L(\mathbf{x}, \dot{\mathbf{x}}, t) dt. \quad (2)$$

We use this formula all along in this article and, because of its perturbative nature, we will also use only formulas up to the third order in time.

The first line of Eq. (1) correspond to the 1D case due to the field gradient  $E'$  and the linear dependence of the potential energy  $E'_p$ . However, in 3D we see extra terms appearing. One of the most important is  $E'_p \frac{E'^2}{8E_0} r^2$ , which occurs even in a pure gradient ( $E'$ ) along  $z$  and a linear potential energy ( $E'_p$ ) studied previously. This illustrates already why the 3D picture is required even to study the simplest “1D case.” Even if the gradient of the field is perfectly homogeneous (and the dependence of the potential energy is linear), some nonlinear terms are present in the Lagrangian. Therefore, even in this ideal case the problem cannot be treated as a 1D problem as done in Refs. [23,24].

More generally, the presence of extra terms will produce (very large) extra phases (see, for instance, the lower panel in Fig. 1), which we thus need to cancel, or control, as much as possible.

### III. ELECTRIC AND MAGNETIC FIELD CANCELLATION

#### A. Cancellation using pure field

Compared to the ideal case, some quadratic and even nonquadratic terms arise. A simple solution would be to cancel these extra terms by an appropriate choice of fields or states. For instance, an appropriate choice of the external field with  $E'' = \frac{E'^2}{2E_0}$  would cancel the  $r^2$  term (and also the  $r^2 z$  term), and an appropriate choice of a state with a potential energy that fits  $E'_p = -\frac{E'_p}{2E_0}$  would cancel the  $z^2$  term. We note that the  $z^3$  term could, in principle, also be canceled by choosing  $E'''_p = -\frac{3E''_p}{2E_0}$ , but because the state, and so its potential energy  $E_p(E)$ , is already partially imposed by the previous equality, we may have not enough degree of freedom for the choice.

Even canceling only the second-order terms seems difficult, because if this requires the equation  $E''_p = -\frac{E'_p}{2E_0}$  to be verified only locally, that is, at field  $E_0$ , we see that if we want to solve it for all possible  $E_0$ , it becomes  $E''_p = -\frac{E'_p}{2E}$  that is solved  $E'_p(E) \propto \sqrt{E}$ . Thus, to cancel the second-order terms the variation of the potential energy should, at least locally at field  $E_0$ , have a kind of a square-root dependence. Unfortunately, Eq. (A1), for (anti-)hydrogen atoms in Rydberg state, indicates that the Stark effect is quite linear. We have indeed checked that the cancellation is impossible for all (anti-)hydrogen states because  $E''_p < -\frac{E'_p}{2E_0}$  for any electric fields below the ionization threshold ( $1/9n^4$  in atomic units for a level with a principal quantum number  $n$ ). Similar behavior exists for the pure magnetic Zeeman effect for low-lying states. We have also checked that it is impossible to get  $E''_p = -\frac{E'_p}{2E_0}$  for the (anti-)hydrogen ground state even if the hyperfine structure is taken into account using the Breit-Rabi formula.

It is, however, interesting to note that the Breit-Rabi formula for nuclear spin value  $I > 1/2$  allows the equality  $E''_p = -\frac{E'_p}{2E_0}$  for sub-Zeeman levels  $m_F < 0$ . In addition, this occurs for the interesting case of  $\tilde{a}_1 \approx -\tilde{a}_2$  for the two  $|F = I \pm 1/2, m_F\rangle$  hyperfine states. For instance, for  $^{87}\text{Rb}$  it arises at  $B = 0.044\,066\,5$  Tesla for both  $|m_F = -1\rangle$  states, and for

$^{85}\text{Rb}$  it arises at  $B = 0.028\,357\,3$  Tesla for both  $m_F = -2$  and at  $B = 0.012\,446\,7$  Tesla for both  $m_F = -1$  [59].

It is beyond the scope of this article to cover all atomic cases including fine, hyperfine, or diamagnetic terms. But the first conclusion concerning the cancellation is that the (anti-)hydrogen atom is peculiar because of its almost linear Stark (and Zeeman) effect. The simplest possibility to cancel the nonlinear terms is thus to combine an electric and a magnetic field to produce locally a square-root dependence of the potential energy curve with the fields. We are going to study this case, which will also include the fact that for Rydberg states the diamagnetic Zeeman effect can play a substantial role [60–64].

#### B. Cancellation using electric and magnetic fields

Combining electric and magnetic fields strongly modifies the curvature of the energy levels and provides some level crossings. Thus this may lead to the cancellation we are looking for. For this study we simply use the (second-order) potential energy formula, Eq. (B1), valid for arbitrary  $\mathbf{B}$  and  $\mathbf{E}$  fields. The eigenstates are noted  $|n, m_1, m_2\rangle$ , with  $m_1, m_2$  quantum numbers spanning  $-(n-1)/2, -(n-3)/2, \dots, (n-1)/2$ .

Several field geometries are possible. We have looked at many of them and found similar results; therefore we illustrate the result using only the simplest case of a constant and uniform magnetic field along the  $z$  axis, in addition to the already studied cylindrical symmetric electric field. This solution is appealing because such a 1–5 Tesla field is naturally present in most of the antihydrogen experiments.

For these fields, the potential energy is calculated using Eq. (B1). We then analytically expand it in series to evaluate the  $E'_p, E''_p$  terms. This leads to the choices (in atomic units)

$$\begin{aligned} E_0 &= 0, \\ \frac{E''}{E^2} &= \frac{n^3(-19 + 12(m_1^2 + m_1 m_2 + m_2^2)) - 17n^2}{12(m_2 - m_1)}, \\ B &= -\frac{12(m_1 + m_2)}{n^2(21 - 20m_1 m_2 + 15n^2)}, \end{aligned}$$

in order to cancel the quadratic terms in the Lagrangian. These choices create a linear potential energy  $E_p = -(3/2)(m_1 - m_2)nE'z$  (up to the second-order terms) for a given  $|n, m_1, m_2\rangle$  state. The third-order terms are *a priori* not canceled.

Cancellation of the second-order nonlinear terms (in  $r^2$  and  $z^2$ ) imposes the value for the magnetic and electric field for a given  $|n, m_1, m_2\rangle$  state. But we have (at least) two states in the interferometer. Thus we have to choose compatible  $|n, m_1, m_2\rangle$  (for state 1 with acceleration  $\tilde{\mathbf{a}}_1$ ) and  $|n', m'_1, m'_2\rangle$  (for state 2 with acceleration  $\tilde{\mathbf{a}}_2$ ) levels that give similar (exact equality was found to be impossible) magnetic and electric fields. So, for instance, we have  $B \approx -\frac{12(m_1+m_2)}{n^2(21-20m_1m_2+15n^2)} \approx -\frac{12(m'_1+m'_2)}{n'^2(21-20m'_1m'_2+15n'^2)}$  and, if possible, we do not create third-order terms that are too high.

Several choices of pairs of states are possible. We found very similar results with many choices, and so we simply mention three of them to express possible and typical values for the interferometric phases:

(i)  $n = 20, m_1 = 13/2, m_2 = -19/2$  and  $n' = 21, m'_1 = -1, m'_2 = -2$  requires similar magnetic fields  $B_0 \approx 2.91$  T and  $E'^2/E''' \approx 200$  V/cm.

(ii)  $n = 19, m_1 = -7, m_2 = 3,$  and  $n' = 20, m'_1 = -17/2, m'_2 = 7/2$  with  $B_0 \approx 5.33$  T and  $E'^2/E''' \approx -160$  V/cm.

(iii)  $n = 18, m_1 = 11/2, m_2 = -17/2$  and  $n' = 37, m'_1 = -18, m'_2 = -15$  with  $B_0 \approx 4.49$  T and  $E'^2/E''' \approx 300$  V/cm.

Because each chosen pair of states leads to results within the same order of magnitude of the final phases, we give here the results using only the third (last) choice.

In order to quickly estimate the contrast of the interferometer, we calculate the phase evolution for 16 particles with two different initial positions in  $z$ , two different initial positions in  $r$ , two different initial velocities along  $z$ , and two different initial velocities along  $r$ . We compare the phase with that arising from a particle starting at the center and with zero initial velocity. We finally average the absolute values of all phases. We use a typical (axial  $z$  and radial  $r$ ) distance of 1 mm and axial and radial thermal velocities corresponding at an initial temperature of  $T_0 = 0.01$  K [ $\sqrt{k_B T_0/m} \approx 10$  m/s for the (anti-)hydrogen mass]. This temperature is chosen because it is reachable with laser-cooling methods, and higher temperatures start to create too much dephasing; lower temperatures do not really help because the dephasing is no longer dominated by the velocity but by other effects such as the third-order terms in the Lagrangian.

The cubic dependence of the phase with the evolution time favors long evolution times. However, in order to keep dephasing (due to imperfect cancellation of second- and third-order terms in the Lagrangian for both states simultaneously) smaller than  $2\pi$  we are restricted to an evolution time (between light pulses) of  $T/4 = 100$   $\mu$ s. We choose an electric field gradient of  $E' = 10$  V/cm<sup>2</sup>. It cannot be much larger, to avoid dephasing terms which are too big, and it cannot be much smaller, because this is what creates the opening of the area of the interferometer and thus the enhancement effect we are looking for. For our gradient interferometer we find a total (global) phase of  $\phi = 472\,808$  ( $\phi \propto E'^2 m^{-1} T^3$ ). This indicates that, as previously stated, a field stability and geometric homogeneity on the order of  $10^{-5}$  is probably required in order to avoid a complete blurring of the fringes (meaning a fluctuation of this phase value of less than  $2\pi$ ). Unfortunately, the interesting term linked to gravity  $2\frac{m}{\hbar}g(a_2 - a_1)T^3$  is only 85.85 (this term is proportional to  $E'm^0T^3$ ). Therefore the gain (factor  $\sim 30$ ) compared to a simple Kasevich-Chu phase of  $kgT^2 = 3.08$  [calculated with a quite arbitrary choice of  $k = (2\pi)/(200$  nm)] can be seen as marginal compared to the optimistic value expected at the beginning of this article. Finally, the (error) phase due to second- and third-order terms is indeed small (0.3) and will probably not create too bad of a contrast.

#### IV. CONCLUSION

We have shown that using a pure gradient of electric or magnetic field in order to produce strong forces able to

increase the area of an interferometer, which seems attractive when looking on a 1D picture, turns out to be quite complicated in a real 3D picture. Despite the field stability issues, the other limitations are first, a pure gradient along one axis is not possible due to zeros of the field divergence in Maxwell's equation, and second, the extra terms produced are difficult to cancel using pure fields for (anti-)hydrogen atoms. We nevertheless note that for ground-state alkali atoms the Breit-Rabi formula allows this cancellation for specific magnetic field values, which might be interesting to study.

Combining electric and magnetic fields helps but has many drawbacks (in addition to the technical difficulty!) because the cancellation is not perfect, implying a choice of given field values and geometries as well as a choice of proper states. Furthermore, the gain we found was quite marginal, at best a factor of 100 compared to a simple Kasevich-Chu's interferometer (with  $N = 1$ ). We have studied only some particular field geometries and pulse sequences, but we doubt that other geometries, time sequences, or even time-dependant fields would lead to drastically better results.

In conclusion, we do not see any strong advantages for use of enhanced interferometers compared to standard ones for precision measurements. We therefore did not discuss in detail the practical implementation of such an interferometer. It is nevertheless worth mentioning that matter-wave interferometry with hydrogen atoms in Rydberg states has been already demonstrated in [65] (by coupling  $2s$  and  $15p$  levels) and that an interferometer using only high Rydberg states has also recently been demonstrated [66,67]. We simply mention that one advantage of such a scheme, using Rydberg states, is that rf or microwave pulses can be used that are easy to implement and can address more velocity classes (due to the reduced Doppler effect) than Raman laser pulses. Therefore it still might be of interest for antimatter experiments to consider such schemes.

We finally mention one possibility to improve the result. We have used perturbation methods for the fields and for the potential energy to study the problem, but it is possible that strong nonlinear terms can be more efficient. We can think of such strong second-order terms that it would lead to trapping of the particles and, as after one oscillation period in a pure harmonic trap, the interferometer can even be closed. This might lead to interesting interferometric measurements that might deserve more study.

#### ACKNOWLEDGMENT

We thank J. Robert, P. Cheinet, and P. Yzombard for fruitful discussions.

#### APPENDIX A: STARK EFFECT

In an electric field  $F$ , neglecting the fine-structure effects that are small for Rydberg states, the energy of states  $E = E_{n,n_1,n_2,m}$  can be accurately calculated from the fourth-order expansion of the hydrogen Stark [63,68–70] states in

atomic units:

$$\begin{aligned}
E = & -\frac{1}{2n^2} + \frac{3n}{2}kF \\
& -\frac{n^4}{16}(17n^2 - 3k)^2 - 9m^2 + 19)F^2 \\
& + \frac{3n^7}{32}k(23n^2 - k^2 + 11m^2 + 39)F^3 \\
& - \frac{n^{10}}{1024}(5487n^4 + 35182n^2 - 1134m^2k^2 \\
& + 1806n^2k^2 - 3402n^2m^2 + 147k^4 \\
& - 549m^4 + 5754k^2 - 8622m^2 + 16211)F^4, \quad (\text{A1})
\end{aligned}$$

where  $n = n_1 + n_2 + |m| + 1$  and  $k = n_1 - n_2 = 2n_1 - n - |m|$ . Back to SI units ( $4.36 \times 10^{-18}\text{J}$  for the energy and  $5.14 \times 10^{11}\text{V/m}$  for the field), the acceleration that can be created in an electric field  $F$  is on the order of  $ma \sim 4.36 \times 10^{-18}\text{J} \frac{3}{2}n^2 \frac{\nabla F}{5.14 \times 10^{11}\text{V/m}}$ .

## APPENDIX B: STARK-ZEEMAN EFFECT

The energy levels of a hydrogen atom in electric and magnetic fields with arbitrary orientation have been studied [71] and analytical formulas up to second order in the fields have been calculated [72]. The states are labeled  $|nn'n''\rangle$ ; they correspond when  $E = 0$  to the  $|nn_1n_2m\rangle$  Stark states with  $n' = (m + n_2 - n_1)/2$  and  $n'' = (m - n_2 + n_1)/2$  [73,74]. In atomic units [ $f = F/(5.14 \times 10^9\text{V/cm})$ ,  $\gamma = B/(2.35 \times 10^5\text{T})$ ] we have

$$\begin{aligned}
E_p = & -\frac{1}{2n^2} + |\omega_1|n' + |\omega_2|n'' \\
& -\frac{n^4 f^2}{16}\{17n^2 + 19 - 12[n^2 + n'n'' \cos(\alpha_1 + \alpha_2) + n''^2]\} \\
& + \frac{n^2 \gamma^2}{48}\{7n^2 + 5 + 4n'n'' \sin \alpha_1 \sin \alpha_2\} \\
& + (n^2 - 1)(\cos^2 \alpha_1 + \cos^2 \alpha_2) \\
& - 12(n^2 \cos^2 \alpha_1 - n'n'' \cos \alpha_1 \cos \alpha_2 \\
& + n''^2 \cos^2 \alpha_2), \quad (\text{B1})
\end{aligned}$$

where  $\omega_{1,2} = \frac{1}{2}(\gamma \mp 3nf)$ , and  $\alpha_1$  and  $\alpha_2$  are the angles between the magnetic field axis and the vectors  $\omega_1$  and  $\omega_2$ , respectively.

## APPENDIX C: PHASE EVOLUTION IN INTERFEROMETERS

We recall here the basics of the calculation of the evolution of the atomic wave packet in our simple two-path atom interferometer. We will deal with nonrelativistic atom interferometry (see [75] for a more general case). Several methods exist to study the evolution: using a plane wave or a Gaussian wave-packet decomposition [76,77], sometimes linked with a path integrals formulation [8,9], or using the density matrix [78] or Wigner function evolution [57,79–82]. Obviously, all methods lead to the same final results, but the choice is made depending on the context.

The most important results concern the case of the (laser-free) evolution under a Hamiltonian (or a Lagrangian) containing a potential that is at most quadratic in the space coordinates. That is when each internal state  $|1\rangle, |2\rangle, \dots$  evolves under its own Hamiltonian  $H_1, H_2, \dots$  that contains only a homogeneous acceleration and its gradient. This is, for instance, the case for the first two lines of Eq. (1). Under such circumstances, that fortunately are the most usual ones, the quantum phase-space (Wigner) distribution evolves under the same (Liouville's) equation than the classical phase-space distribution [82,86]. The fact that the evolution is given by the classical evolution is also directly visible using the evolution operator between the times  $t_i$  and  $t_f$  that, in the two-level case  $\hat{U}(t_i, t_f) = \begin{pmatrix} U_{11}(t_i, t_f) & 0 \\ 0 & U_{22}(t_i, t_f) \end{pmatrix}$ , is given in the position representation (here written in 1D to simplify the notations) by  $\langle z_f | \hat{U}_{11}(t_i, t_f) | z_i \rangle = \sqrt{\frac{m}{2i\pi\hbar(t_f - t_i)}} e^{iS_{\text{cl}}(z_f, t_f; z_i, t_i)/\hbar}$ , where  $S_{\text{cl}}$  is the classical action evolution of a particle in state  $|1\rangle$ , starting at position  $z_i$  at time  $t_i$  under the forces created by  $H_1$  and arriving at time  $t_f$  at position  $z_f$ . In other words, the phase evolution of the wave function is given by the (semiclassical limit of the) Feynman's path-integral formulation in terms of the Lagrangian by

$$\phi = \frac{S_{\text{cl}}}{\hbar} = \frac{1}{\hbar} \int_{\Gamma} L(\mathbf{x}, \dot{\mathbf{x}}, t) dt, \quad (\text{C1})$$

and  $\Gamma$  is the classical path from the initial to the final point. This was first proposed by Kennard and Van Vleck [83,84] and shown by Morette [85] to be exact in the quadratic case.

In our case, we also deal with higher-order terms, such as the third-order terms ( $r^2z$  and  $z^3$ ). The theory is more complex and generally no longer linked to the classical world with, for instance, negative values for the Wigner function [82,86]. Fortunately, if the extra terms are considered as a perturbation  $L_1$  on the Lagrangian  $L = L_0 + L_1$ , the phase shift  $\delta\phi$  introduced into the final wave function, by the perturbation  $L_1$ , is given simply (to the first order) by the integral of the perturbation along the classical unperturbed path  $\Gamma_0$  [87–89]:

$$\delta\phi = \frac{1}{\hbar} \int_{\Gamma_0} L_1 dt. \quad (\text{C2})$$

This allows one to calculate the phases created by the accelerations.

We should also deal with the  $\pi$  or  $\pi/2$  light pulses. The general case of the interaction with lights can be complicated, because correlations may appear between internal and external variables invalidating the Bloch equation or the simple semiclassical approaches [82,86]. However, because it is not the main focus of our article to deal with these issues, we will restrict ourselves to the ideal case of a quasi-instantaneous light pulse and with no momentum transfer created by the pulses. This can be realized, for instance, thanks to the use of copropagating laser Raman beams. Therefore, for  $\pi$  pulse at time  $t_i$  we have  $\hat{U}_{\pi}(t_i) = \begin{pmatrix} 0 & -ie^{i\phi_L(t_i)} \\ -ie^{-i\phi_L(t_i)} & 0 \end{pmatrix}$ . Similarly, the evolution under a  $\pi/2$  pulse is given by  $\hat{U}_{\pi/2}(t_i) = \frac{1}{\sqrt{2}} \begin{pmatrix} 1 & -ie^{i\phi_L(t_i)} \\ -ie^{-i\phi_L(t_i)} & 1 \end{pmatrix}$ . In these formulas  $\phi_L(t_i)$  is the laser phase at time  $t_i$  [or the phase difference  $\phi_L(t_i) = \phi_{L_1}(t_i) - \phi_{L_2}(t_i)$  in the case of two Raman laser beams].

In conclusion, by multiplying the matrix evolution we can calculate the state evolution. In our case of simple (upper  $u$  and lower  $l$ ) paths with the two internal states, if starting (for instance) with atoms in state  $|1\rangle$ , we find that the probability to observe atoms in state  $|1\rangle$  just after the last  $\pi/2$  pulse is

$$P = \frac{1}{2}[1 - C \cos(\phi_u - \phi_l + \phi_L)],$$

where  $\phi_u$ , respectively  $\phi_l$ , is the phase acquired by the particles in the upper, respectively lower branch (with possible internal state change during the motion).  $\phi_L$  comes from the phases imprinted by the lasers. For a single atom the contrast  $C = 1$ , but obviously when summed over all initial atomic

phase-space densities, the dephasing and the incoherent sums of the probabilities lead to a reduction of the contrast. A simple case is when the initial wave packet ( $|\psi_0\rangle$  in the pure case) or the initial phase-space distribution (in the statistical ensemble case) is Gaussian and the evolution is quadratic. In such a case, as shown before, the position-momentum mean and (co-)variance evolves in a very simple analytical manner given by the classical evolution (in the so-called ABCD  $\xi$  theorem) [57,76,77,79–81], directly giving the final contrast (using obvious notations)  $Ce^{i\phi} = \langle \psi_0 | \hat{U}_u^\dagger \hat{U}_l | \psi_0 \rangle = \langle \psi_u | \psi_l \rangle = \int \psi_u^*(z) \psi_l(z) dz$ . However, our case is more complex, with nonquadratic terms in the Hamiltonian. No analytical formulas exist, and we therefore simply estimate the loss of contrast, or dephasing, by calculating the phases for several different initial position-momentum states.

- 
- [1] R. Colella, A. W. Overhauser, and S. A. Werner, Observation of Gravitationally Induced Quantum Interference, *Phys. Rev. Lett.* **34**, 1472 (1975).
- [2] M. K. Oberthaler, Anti-matter wave interferometry with positronium, *Nucl. Instrum. Methods Phys. Res., Sect. B* **192**, 129 (2002).
- [3] P. Hamilton, A. Zhmoginov, F. Robicheaux, J. Fajans, J. S. Wurtele, and H. Müller, Antimatter Interferometry for Gravity Measurements, *Phys. Rev. Lett.* **112**, 121102 (2014).
- [4] A. Kellerbauer, M. Amoretti, A. S. Belov, G. Bonomi, I. Boscolo, R. S. Brusa, M. Büchner, V. M. Byakov, L. Cabaret, C. Canali, C. Carraro, F. Castelli, S. Cialdi, M. de Combarieu, D. Comparat, G. Consolati, N. Djourelou, M. Doser, G. Drobychev, A. Dupasquier *et al.*, Proposed antimatter gravity measurement with an antihydrogen beam, *Nucl. Instrum. Methods Phys. Res., Sect. B* **266**, 351 (2008).
- [5] S. Sala, F. Castelli, M. Giammarchi, S. Siccardi, and S. Olivares, Matter-wave interferometry: Towards antimatter interferometers, *J. Phys. B: At., Mol. Opt. Phys.* **48**, 195002 (2015).
- [6] S. Sala, M. Giammarchi, and S. Olivares, Asymmetric Talbot-Lau interferometry for inertial sensing, *Phys. Rev. A* **94**, 033625 (2016).
- [7] Ch J. Bordé, Atomic interferometry with internal state labeling, *Phys. Lett. A* **140**, 10 (1989).
- [8] M. Kasevich and S. Chu, Atomic Interferometry Using Stimulated Raman Transitions, *Phys. Rev. Lett.* **67**, 181 (1991).
- [9] A. D. Cronin, J. Schmiedmayer, and D. E. Pritchard, Optics and interferometry with atoms and molecules, *Rev. Mod. Phys.* **81**, 1051 (2009).
- [10] S. Abend, M. Gersemann, C. Schubert, D. Schlippert, E. M. Rasel, M. Zimmermann, M. A. Efremov, A. Roura, F. A. Narducci, and W. P. Schleich, Atom interferometry and its applications, *Found. Quantum Theory* **197**, 345 (2019).
- [11] K. Hornberger, S. Gerlich, H. Ulbricht, L. Hackermüller, S. Nimmrichter, I. V. Goldt, O. Boltalina, and M. Arndt, Theory and experimental verification of Kapitza-Dirac-Talbot-Lau interferometry, *New J. Phys.* **11**, 043032 (2009).
- [12] B. Brezger, L. Hackermüller, S. Uttenthaler, J. Petschinka, M. Arndt, and A. Zeilinger, Matter-Wave Interferometer for Large Molecules, *Phys. Rev. Lett.* **88**, 100404 (2002).
- [13] S. Gerlich, L. Hackermüller, K. Hornberger, A. Stibor, H. Ulbricht, M. Gring, F. Goldfarb, T. Savas, M. Müri, M. Mayor *et al.*, A Kapitza-Dirac-Talbot-Lau interferometer for highly polarizable molecules, *Nat. Phys.* **3**, 711 (2007).
- [14] J. M. McGuirk, M. J. Snadden, and M. A. Kasevich, Large Area Light-Pulse Atom Interferometry, *Phys. Rev. Lett.* **85**, 4498 (2000).
- [15] S.-W. Chiow, T. Kovachy, H.-C. Chien, and M. A. Kasevich, 102 $\hbar$ k Large Area Atom Interferometers, *Phys. Rev. Lett.* **107**, 130403 (2011).
- [16] H. Müller, Sheng-wei Chiow, Quan Long, Sven Herrmann, and Steven Chu, Atom Interferometry with up to 24-Photon-Momentum-Transfer Beam Splitters, *Phys. Rev. Lett.* **100**, 180405 (2008).
- [17] H. Müller, S.-W. Chiow, S. Herrmann, and S. Chu, Atom Interferometers with Scalable Enclosed Area, *Phys. Rev. Lett.* **102**, 240403 (2009).
- [18] P. Cladé, S. Guellati-Khélifa, F. Nez, and F. Biraben, Large Momentum Beam Splitter Using Bloch Oscillations, *Phys. Rev. Lett.* **102**, 240402 (2009).
- [19] K. Kotru, D. L. Butts, J. M. Kinast, and R. E. Stoner, Large-Area Atom Interferometry with Frequency-Swept Raman Adiabatic Passage, *Phys. Rev. Lett.* **115**, 103001 (2015).
- [20] S. Machluf, Y. Japha, and R. Folman, Coherent Stern-Gerlach momentum splitting on an atom chip, *Nat. Commun.* **4**, 2424 (2013).
- [21] G. D. McDonald, C. C. N. Kuhn, S. Bennetts, J. E. Debs, K. S. Hardman, J. D. Close, and N. P. Robins, A faster scaling in acceleration-sensitive atom interferometers, *Europhys. Lett.* **105**, 63001 (2014).
- [22] Y. Margalit, Z. Zhou, O. Dobkowsky, Y. Japha, D. Rohrlich, S. Moukouri, and R. Folman, Realization of a complete Stern-Gerlach interferometer, [arXiv:1801.02708](https://arxiv.org/abs/1801.02708).
- [23] O. Amit, Y. Margalit, O. Dobkowsky, Z. Zhou, Y. Japha, M. Zimmermann, M. A. Efremov, F. A. Narducci, E. M. Rasel, W. P. Schleich *et al.*,  $T^3$  Stern-Gerlach Matter-Wave Interferometer, *Phys. Rev. Lett.* **123**, 083601 (2019).
- [24] M. Zimmermann, M. A. Efremov, A. Roura, W. P. Schleich, S. A. DeSavage, J. P. Davis, A. Srinivasan, F. A. Narducci, S. A. Werner, and E. M. Rasel,  $T^3$ -interferometer for atoms, *Appl. Phys. B* **123**, 102 (2017).

- [25] Y. Margalit, Z. Zhou, S. Machluf, Y. Japha, S. Moukouri, and R. Folman, Analysis of a high-stability Stern–Gerlach spatial fringe interferometer, *New J. Phys.* **21**, 073040 (2019).
- [26] E. P. Liang and C. D. Dermer, Laser cooling of positronium, *Opt. Commun.* **65**, 419 (1988).
- [27] I. D. Setija, H. G. C. Werij, O. J. Luiten, M. W. Reynolds, T. W. Hijmans, and J. T. M. Walraven, Optical Cooling of Atomic Hydrogen in a Magnetic Trap, *Phys. Rev. Lett.* **70**, 2257 (1993).
- [28] J. K. Stockton, K. Takase, and M. A. Kasevich, Absolute Geodetic Rotation Measurement Using Atom Interferometry, *Phys. Rev. Lett.* **107**, 133001 (2011).
- [29] I. Dutta, D. Savoie, B. Fang, B. Venon, C. L. Garrido Alzar, R. Geiger, and A. Landragin, Continuous Cold-Atom Inertial Sensor with 1 nrad/sec Rotation Stability, *Phys. Rev. Lett.* **116**, 183003 (2016).
- [30] A. Peters, K. Y. Chung, and S. Chu, High-precision gravity measurements using atom interferometry, *Metrologia* **38**, 25 (2001).
- [31] G. W. Biedermann, X. Wu, L. Deslauriers, S. Roy, C. Mahadeswaraswamy, and M. A. Kasevich, Testing gravity with cold-atom interferometers, *Phys. Rev. A* **91**, 033629 (2015).
- [32] C. Amole, M. D. Ashkezari, M. Baquero-Ruiz, W. Bertsche, E. Butler, A. Capra, C. L. Cesar, M. Charlton, S. Eriksson, J. Fajans *et al.*, Description and first application of a new technique to measure the gravitational mass of antihydrogen, *Nat. Commun.* **4**, 2787 (2013).
- [33] Jiafeng Cui, Yaoyao Xu, Lele Chen, Kun Qi, Minkang Zhou, Xiaochun Duan, and Zhongkun Hu, Time base evaluation for atom gravimeters, *Rev. Sci. Instrum.* **89**, 083104 (2018).
- [34] R. Karcher, A. Imanaliev, S. Merlet, and F. Pereira Dos Santos, Improving the accuracy of atom interferometers with ultracold sources, *New J. Phys.* **20**, 113041 (2018).
- [35] M. Kritsotakis, S. S. Szigeti, J. A. Dunningham, and S. A. Haine, Optimal matter-wave gravimetry, *Phys. Rev. A* **98**, 023629 (2018).
- [36] K. Bongs, M. Holynski, J. Vovrosh, P. Bouyer, G. Condon, E. Rasel, C. Schubert, W. P. Schleich, and A. Roura, Taking atom interferometric quantum sensors from the laboratory to real-world applications, *Nat. Rev. Phys.* **1**, 731 (2019).
- [37] Z. Fu, B. Wu, B. Cheng, Y. Zhou, K. Weng, D. Zhu, Z. Wang, and Q. Lin, A new type of compact gravimeter for long-term absolute gravity monitoring, *Metrologia* **56**, 025001 (2019).
- [38] Y. Yamazaki and S. Ulmer, CPT symmetry tests with cold  $\bar{p}$  and antihydrogen, *Ann. Phys.* **525**, 493 (2013).
- [39] M. Hori and J. Walz, Physics at CERN’s antiproton decelerator, *Prog. Part. Nucl. Phys.* **72**, 206 (2013).
- [40] K. Kirch and K. S. Khaw, Testing antimatter gravity with muonium, *Int. J. Mod. Phys. Conf. Ser.* **30**, 1460258 (2014).
- [41] V. A. Kostelecký and A. J. Vargas, Lorentz and CPT tests with hydrogen, antihydrogen, and related systems, *Phys. Rev. D* **92**, 056002 (2015).
- [42] M. S. Safronova, D. Budker, D. DeMille, D. F. J. Kimball, A. Derevianko, and C. W. Clark, Search for new physics with atoms and molecules, *Rev. Mod. Phys.* **90**, 025008 (2018).
- [43] R. Poggiani, A possible gravity measurement with antihydrogen, *Hyperfine Interact.* **76**, 371 (1993).
- [44] R. Poggiani, Measurement of the gravitational acceleration of antihydrogen, *Hyperfine Interact.* **109**, 367 (1997).
- [45] A. P. Mills and M. Leventhal, Can we measure the gravitational free fall of cold Rydberg state positronium? *Nucl. Instrum. Methods Phys. Res., Sect. B* **192**, 102 (2002).
- [46] J. Walz and T. W. Hänsch, A proposal to measure antimatter gravity using ultracold antihydrogen atoms, *Gen. Relativ. Gravitation* **36**, 561 (2004).
- [47] P. Perez and A. Rosowsky, A new path toward gravity experiments with antihydrogen, *Nucl. Instrum. Methods Phys. Res., Sect. A* **545**, 20 (2005).
- [48] D. B. Cassidy and S. D. Hogan, Atom control and gravity measurements using Rydberg positronium, *Int. J. Mod. Phys.: Conf. Ser.* **30**, 1460259 (2014).
- [49] P. Perez, D. Banerjee, F. Biraben, D. Brook-Roberge, M. Charlton, P. Cladé, P. Comini, P. Crivelli, O. Dalkarov, P. Debu *et al.*, The GBAR antimatter gravity experiment, *Hyperfine Interact.* **233**, 21 (2015).
- [50] P. Crivelli, D. A. Cooke, and S. Friedreich, Experimental considerations for testing antimatter antigravity using positronium 1S-2S spectroscopy, *Int. J. Mod. Phys.: Conf. Ser.* **30**, 1460257 (2014).
- [51] T. J. Phillips, A technique for directly measuring the gravitational acceleration of antihydrogen, in *Low Energy Antiproton Physics, Proceedings of the Third Biennial Conference, Bled, Slovenia, 1994*, edited by G. Kernel, P. Krian, and M. Miku (World Scientific Publishing Company, Singapore, 1995), p. 569.
- [52] T. J. Phillips, Measuring the gravitational acceleration of antimatter with an antihydrogen interferometer, *Hyperfine Interact.* **100**, 163 (1996).
- [53] T. J. Phillips, Antimatter gravity studies with interferometry, *Hyperfine Interact.* **109**, 357 (1997).
- [54] Byung Jin Chang, R. Alferness, and E. N. Leith, Space-invariant achromatic grating interferometers: Theory, *Appl. Opt.* **14**, 1592 (1975).
- [55] M. W. Horbatsch, M. Horbatsch, and E. A. Hessels, A universal formula for the accurate calculation of hydrogenic lifetimes, *J. Phys. B* **38**, 1765 (2005).
- [56] B. Barrett, A. Bertoldi, and P. Bouyer, Inertial quantum sensors using light and matter, *Phys. Scr.*, **91**, 053006 (2016).
- [57] M. Zimmermann, M. A. Efremov, W. Zeller, W. P. Schleich, J. P. Davis, and F. A. Narducci, Representation-free description of atom interferometers in time-dependent linear potentials, *New J. Phys.* **21**, 073031 (2019).
- [58] J. Orloff, *Handbook of Charged Particle Optics* (CRC Press, Boca Raton, FL, 2008).
- [59] D. A. Steck, <http://steck.us/alkalidata>.
- [60] T. F. Gallagher, *Rydberg Atoms* (Cambridge University Press, Cambridge, UK, 1994).
- [61] H. Friedrich and H. Wintgen, The hydrogen atom in a uniform magnetic field—An example of chaos, *Phys. Rep.* **183**, 37 (1989).
- [62] J. Pinard, Atoms in static electric and magnetic fields: The experimental aspect, *Atoms in Strong Fields* (Springer, New York, 1990), pp. 17–42.
- [63] V. S. Lisitsa, New results on the Stark and Zeeman effects in the hydrogen atom, *Sov. Phys. Usp.* **30**, 927 (1987).



- [64] T. Bartsch and T. Uzer, *Rydberg Atoms in Strong Static Fields* (Springer, New York, 2006), pp. 274–252.
- [65] T. Heupel, M. Mei, M. Niering, B. Gross, M. Weitz, T. W. Hänsch, and Ch. J. Bordé, Hydrogen atom interferometer with short light pulses, *Europhys. Lett.* **57**, 158 (2002).
- [66] J. E. Palmer and S. D. Hogan, Electric Rydberg-Atom Interferometry, *Phys. Rev. Lett.* **122**, 250404 (2019).
- [67] J. E. Palmer and S. D. Hogan, Matter-wave interferometry with atoms in high Rydberg states, *Mol. Phys.* **117**, 3108 (2019).
- [68] H. J. Silverstone, Perturbation theory of the Stark effect in hydrogen to arbitrarily high order, *Phys. Rev. A* **18**, 1853 (1978).
- [69] C. Bordas and H. Helm, Electric-field ionization of Rydberg states of  $H_3$ , *Phys. Rev. A* **47**, 1209 (1993).
- [70] S. D. Hogan, Calculated photoexcitation spectra of positronium Rydberg states, *Phys. Rev. A* **87**, 063423 (2013).
- [71] J. Main, M. Schwacke, and G. Wunner, Hydrogen atom in combined electric and magnetic fields with arbitrary mutual orientations, *Phys. Rev. A* **57**, 1149 (1998).
- [72] E. A. Solovev, Second order perturbation theory for the hydrogen atom in crossed electric and magnetic fields, *Zh. Eksp. Teor. Fiz.* **85**, 109 (1983) [*JETP* **58**, 63 (1983)].
- [73] Yu. N. Demkov, B. S. Monozon, and V. N. Ostrovskii, Energy levels of a hydrogen atom in crossed electric and magnetic fields, *Zh. Eksp. Teor. Fiz.* **57**, 1431 (1970) [*Sov. Phys. JETP* **30**, 775 (1970)].
- [74] V. D. Ovsianikov and S. V. Goossev, Diamagnetic shift and splitting of Rydberg levels in atoms, *Phys. Scr.* **57**, 506 (1998).
- [75] C. J. Bordé, Atom interferometry using internal excitation: Foundations and recent theory, in *International School of Physics Enrico Fermi—COURSE CLXXXVIII Atom Interferometry*, edited by G. M. Tino and M. A. Kasevich (IOS, Amsterdam, Bologna, 2014), pp. 143–170.
- [76] C. J. Bordé, Theoretical tools for atom optics and interferometry, *C.R. Acad. Sci., Ser. IV: Phys.*, **2**, 509 (2001).
- [77] Ch. Antoine and Ch. J. Bordé, Quantum theory of atomic clocks and gravito-inertial sensors: An update, *J. Opt. B: Quantum Semiclassical Opt.* **5**, S199 (2003).
- [78] B. Dubetsky and M. A. Kasevich, Atom interferometer as a selective sensor of rotation or gravity, *Phys. Rev. A* **74**, 023615 (2006).
- [79] A. Roura, W. Zeller, and W. P. Schleich, Overcoming loss of contrast in atom interferometry due to gravity gradients, *New J. Phys.* **16**, 123012 (2014).
- [80] S. Kleinert, E. Kajari, A. Roura, and W. P. Schleich, Representation-free description of light-pulse atom interferometry including non-inertial effects, *Phys. Rep.* **605**, 1 (2015).
- [81] A. Roura, Circumventing Heisenberg’s Uncertainty Principle in Atom Interferometry Tests of the Equivalence Principle, *Phys. Rev. Lett.* **118**, 160401 (2017).
- [82] T. Chanelière, D. Comparat, and H. Lignier, Phase-space-density limitation in laser cooling without spontaneous emission, *Phys. Rev. A* **98**, 063432 (2018).
- [83] E. H. Kennard, Zur quantenmechanik einfacher bewegungstypen, *Z. Phys. A* **44**, 326 (1927).
- [84] J. H. Van Vleck, The correspondence principle in the statistical interpretation of quantum mechanics, *Proc. Natl. Acad. Sci.* **14**, 178 (1928).
- [85] C. Morette, On the definition and approximation of Feynman’s path integrals, *Phys. Rev.* **81**, 848 (1951).
- [86] W. B. Case, Wigner functions and Weyl transforms for pedestrians, *Am. J. Phys.* **76**, 937 (2008).
- [87] P. Storey and C. Cohen-Tannoudji, The Feynman path integral approach to atomic interferometry, A tutorial, *J. Phys. II* **4**, 1999 (1994).
- [88] K. Bongs, R. Launay, and M. A. Kasevich, High-order inertial phase shifts for time-domain atom interferometers, *Appl. Phys. A* **84**, 599 (2006).
- [89] A. Bertoldi, F. Minardi, and M. Prevedelli, Phase shift in atom interferometers: Corrections for nonquadratic potentials and finite-duration laser pulses, *Phys. Rev. A* **99**, 033619 (2019).